The Astrophysical Journal Letters, 971:L32 (11pp), 2024 August 20 https://doi.org/10.3847/2041-8213/ad6908


# Discovery of an Apparent Red, High-velocity Type Ia Supernova at z = 2.9 with JWST

J. D. R. Pierel[1,18], M. Engesser[1], D. A. Coulter[1], C. DeCoursey[2], M. R. Siebert[1], A. Rest[1,3], E. Egami[2], W. Chen[4], O. D. Fox[1], D. O. Jones[5], B. A. Joshi[3], T. J. Moriya[6,7,8], Y. Zenati[1,3,19], A. J. Bunker[9], P. A. Cargile[10], M. Curti[11], D. J. Eisenstein[10], S. Gezari[1], S. Gomez[1], M. Guolo[3], B. D. Johnson[10], M. Karmen[3], R. Maiolino[12,13,14], R. M. Quimby[15,16], B. Robertson[17], M. Shahbandeh[1], L. G. Strolger[1], F. Sun[10], Q. Wang[3], and T. Wevers[1]

[1] Space Telescope Science Institute, Baltimore, MD 21218, USA; jpierel@stsci.edu
[2] Steward Observatory, University of Arizona, 933 N. Cherry Avenue, Tucson, AZ 85721, USA
[3] Physics and Astronomy Department, Johns Hopkins University, Baltimore, MD 21218, USA
[4] Department of Physics, Oklahoma State University, 145 Physical Sciences Bldg, Stillwater, OK 74078, USA
[5] Institute for Astronomy, University of Hawai'i, 640 N. A'ohoku Pl., Hilo, HI 96720, USA
[6] National Astronomical Observatory of Japan, National Institutes of Natural Sciences, 2-21-1 Osawa, Mitaka, Tokyo 181-8588, Japan
[7] Graduate Institute for Advanced Studies, SOKENDAI, 2-21-1 Osawa, Mitaka, Tokyo 181-8588, Japan
[8] School of Physics and Astronomy, Monash University, Clayton, Victoria 3800, Australia
[9] Department of Physics, University of Oxford, Denys Wilkinson Building, Keble Road, Oxford OX1 3RH, UK
[10] Center for Astrophysics | Harvard & Smithsonian, 60 Garden St., Cambridge, MA 02138, USA
[11] European Southern Observatory, Karl-Schwarzschild-Strasse 2, 85748 Garching, Germany
[12] Kavli Institute for Cosmology, University of Cambridge, Madingley Road, Cambridge CB3 0HA, UK
[13] Cavendish Laboratory, University of Cambridge, 19 JJ Thomson Avenue, Cambridge CB3 0HE, UK
[14] Department of Physics and Astronomy, University College London, Gower Street, London WC1E 6BT, UK
[15] Department of Astronomy/Mount Laguna Observatory, SDSU, 5500 Campanile Drive, San Diego, CA 92812-1221, USA
[16] Kavli Institute for the Physics and Mathematics of the Universe (WPI), The University of Tokyo Institutes for Advanced Study, The University of Tokyo, Kashiwa, Chiba 277-8583, Japan
[17] Department of Astronomy & Astrophysics, University of California, Santa Cruz, 1156 High Street, Santa Cruz, CA 96054, USA
*Received 2024 June 7; revised 2024 July 29; accepted 2024 July 29; published 2024 August 13*

## Abstract

We present the James Webb Space Telescope (JWST) discovery of SN 2023adsy, a transient object located in a host galaxy JADES-GS+53.13485−27.82088 with a host spectroscopic redshift of $2.903 \pm 0.007$. The transient was identified in deep (JWST)/NIRCam imaging from the JWST Advanced Deep Extragalactic Survey (JADES) program. Photometric and spectroscopic follow-up with NIRCam and NIRSpec, respectively, confirm the redshift and yield UV-NIR light-curve, NIR color, and spectroscopic information all consistent with a Type Ia classification. Despite its classification as a likely SN Ia, SN 2023adsy is both fairly red ($c \sim 0.9$) despite a host galaxy with low extinction and has a high Ca II velocity ($19{,}000 \pm 2000$ km s$^{-1}$) compared to the general population of SNe Ia. While these characteristics are consistent with some Ca-rich SNe Ia, particularly SN 2016hnk, SN 2023adsy is intrinsically brighter than the low-$z$ Ca-rich population. Although such an object is too red for any low-$z$ cosmological sample, we apply a fiducial standardization approach to SN 2023adsy and find that the SN 2023adsy luminosity distance measurement is in excellent agreement ($\lesssim 1\sigma$) with ΛCDM. Therefore unlike low-$z$ Ca-rich SNe Ia, SN 2023adsy is standardizable and gives no indication that SN Ia standardized luminosities change significantly with redshift. A larger sample of distant SNe Ia is required to determine if SN Ia population characteristics at high $z$ truly diverge from their low-$z$ counterparts and to confirm that standardized luminosities nevertheless remain constant with redshift.

*Unified Astronomy Thesaurus concepts:* Cosmology (343); High-redshift galaxy clusters (2007); Type Ia supernovae (1728); Supernovae (1668)

## 1. Introduction

Type Ia supernovae (SNe Ia) have now been used for decades as precise luminosity distance measures, enabling the discovery of dark energy and our best local measurement of the Hubble constant ($H_0$; Riess et al. 1998; Perlmutter et al. 1999; Riess et al. 2022). SNe Ia can be found over a wide redshift range, making them an ideal tool for measuring changes in dark energy over time. However, doing so requires (1) a large sample of well-observed SNe Ia and (2) that the standardization properties of SNe Ia do not change with redshift. This second point is particularly important, as many redshift-evolving global properties could plausibly impact SN Ia luminosities and mimic the signal of evolving dark energy (e.g., metallicity; Moreno-Raya et al. 2016). This effect could bias dark energy measurements below the level of our current measurement precision (Riess & Livio 2006; Scolnic et al. 2018; Brout et al. 2022).

The exact nature of dark energy is one of the fundamental questions for cosmology, and next-generation SN Ia dark energy measurements will rely upon SN Ia luminosities remaining constant with redshift to remain unbiased. Evolving luminosity distances could indicate dark energy and/or SN Ia

[18] NASA Einstein Fellow.
[19] ISEF International Fellowship.

intrinsic luminosity are changing with redshift, making it difficult to distinguish between the two effects. In the dark matter-dominated universe beyond $z \sim 2$, dark energy variation is expected to be very small, and so evolution in luminosity distances would strongly indicate intrinsic SN Ia luminosity evolution, giving high-$z$ SNe Ia unique leverage on SN Ia systematics (Riess & Livio 2006).

Distance measurements for SNe Ia have been made to $z = 2.22$ with the Hubble Space Telescope (HST; Rodney et al. 2014), but considering only spectroscopically confirmed SNe Ia with spectroscopic redshifts that have not been gravitationally lensed (which adds many systematics; see Pierel et al. 2024b), that sample is limited to $z \sim 1.6$ (Riess et al. 2018). There are only five SNe Ia with luminosity distance measurements in the range $1.6 < z < 2.22$, with two gravitationally lensed (Jones et al. 2013; Rubin et al. 2018) and three photometrically classified (Rodney et al. 2014). Two additional spectroscopically confirmed, gravitationally lensed SNe Ia have been found at $z = 1.78$ (Polletta et al. 2023; Chen et al. 2024; Frye et al. 2024; Pascale et al. 2024, Pierel et al. 2024b) and $z = 1.95$ (Pierel et al. 2024c), but they lack luminosity distance measurements. Detecting SNe Ia at $z > 2$ requires deep ($m_{AB} \gtrsim 26$) imaging observations in red ($\gtrsim 1.5\ \mu$m) filters, while spectroscopic confirmation of SNe Ia at $z > 2$ requires similar depths at wavelengths beyond $\sim 2\ \mu$m to identify the characteristic Si II feature (e.g., Filippenko 1997). These combined requirements have been beyond the reach of modern observatories until the launch of the James Webb Space Telescope (JWST). JWST has expanded our view of the universe to remarkable distances, and despite a relatively small field of view it has been highly efficient at detecting rare SNe at high $z$ due to its sensitivity and wavelength coverage (Engesser et al. 2022a, 2022b; DeCoursey et al. 2023a, 2023b, 2023c, Pierel et al. 2024b, 2024c).

A candidate for the most distant SN Ia yet discovered has been found in JWST imaging conducted as part of the JWST Advanced Deep Extragalactic Survey (JADES) program (Eisenstein et al. 2023). JADES observed $\sim 25'^2$ of sky to extreme depths ($m_{AB} > 30$ in 9 filters) in 2022 November and again in 2023 November, giving a sufficiently long baseline to search for transient objects with sensitivity for SNe Ia to $z > 4$. Of the dozens of detected transient objects, one (subsequently named SN 2023adsy and found in the galaxy JADES-GS +53.13485 −27.82088 at R.A. $= 3^h32^m32\overset{s}{.}3647$ decl.$= -27^d49^m15\overset{s}{.}238$) was identified by first-epoch colors, redshift, and luminosity as a possible SN Ia candidate at $z \sim 2.8$. A JWST Director's Discretionary Time (DDT) program was approved to follow up the most interesting transients in the field (Egami et al. 2023), providing two additional imaging epochs and a spectrum for $\sim 10$ SNe including SN 2023adsy, which received a refined spectroscopic redshift of $z = 2.903 \pm 0.007$.

While the overall JADES+DDT observations and SN population analysis are presented in a companion paper (DeCoursey et al. 2024, hereafter D24), here we describe the classification and analysis of SN 2023adsy in detail. We begin by a summary of the observations in Section 2, followed by a description of the classification for SN 2023adsy using both the spectrum and light curve in Section 3. Light-curve fitting and the subsequent standardized distance measurement are completed in Section 4, and we conclude in Section 5 with prospects for the future of high-$z$ SN Ia cosmology and the implications of the new frontier enabled by JWST. In this analysis, we assume a standard flat ΛCDM cosmology with $H_0 = 70\ \mathrm{km\ s^{-1}\ Mpc^{-1}}$, $\Omega_m = 0.315$.

## 2. Summary of Observations

The description of JADES, its observing strategy and the resulting 2022–2023 data products, the method for detecting SNe, and the subsequent DDT program observations are described in detail by D24. Briefly, the initial JADES observations (PID 1180) were taken over the observing window 2022 September 29–October 5, and the second epoch took place between 2023 September 29 and October 3 with an overlap of $25'^2$ and a $5\sigma$ depth of $m_{AB} \sim 30$ in the NIRCam F090W, F115W, F150W, F200W, F277W, F335M, F356W, F410M, and F444W filters. There were also additional visits on 2023 November 15 and 2024 January 1 due to failed observations. A JWST DDT program (PID 6541) was approved to follow the most interesting transients identified with two additional NIRCam visits on 2023 November 28 and 2024 January 1, with the latter visit including seven hours of integration in the NIRSpec (Jakobsen et al. 2022) multiobject spectroscopy (MOS) mode using the microshutter assembly (MSA; Ferruit et al. 2022) and Prism ($R \sim 100$). The MSA provided SN spectra for $\sim 10$ transients, most described in companion papers (e.g., D. Coulter et al. 2024, in preparation; Siebert et al. 2024) as well as a variety of galaxy spectra. Below we describe the data reduction and analysis for SN 2023adsy.

### 2.1. Measuring Photometry

As described in detail by D24, we adopt the point-spread function (PSF) fitting method developed in Pierel et al. (2024b) for measuring photometry on Level 3 (drizzled, I2D) JWSTimages. Unlike their scenario, though, we have a template image for all epochs of SN 2023adsy from the 2022 JADES observations. We therefore first align the Level 2 (CAL) NIRCam images containing SN 2023adsy to the Level 3 template images (I2Ds,[20] in each filter) using the JWST/HST Alignment Tool (`JHAT`; Rest et al. 2023)[21] software and then produce aligned Level 3 images with the JWST pipeline (Bushouse et al. 2022). JHAT improves the relative alignment from $\sim 1$ to $\sim 0.1$ pixels between the epochs. We obtain difference images in all filters using the High Order Transform of PSF and Template Subtraction (Becker 2015)[22]) code (with modifications implemented in the `photpipe` code; Rest et al. 2005), with all short- and long-wavelength (SW and LW, respectively) first-epoch filters shown in Figure 1. We then implement the `space_phot`[23] Level 3 PSF fitting routine from Pierel et al. (2024b) using $5 \times 5$ pixel cutouts and PSF models from `webbpsf`,[24] which are temporally and spatially dependent and include a correction to the infinite aperture flux. These total fluxes, which are in units of $\mathrm{MJy\ sr^{-1}}$, are converted to AB magnitudes using the native pixel scale of each image ($0''.03$/ pix for SW; $0''.06$/ pix for LW). The measured photometry is given in Table 1.

### 2.2. NIRSpec Reduction

We began processing the spectroscopic data with Stage 2 products from the Mikulski Archive for Space Telescopes (MAST). Additional processing used the JWST pipeline (v

[20] https://archive.stsci.edu/hlsp/jades
[21] https://jhat.readthedocs.io
[22] https://github.com/acbecker/hotpants
[23] space-phot.readthedocs.io
[24] https://webbpsf.readthedocs.io

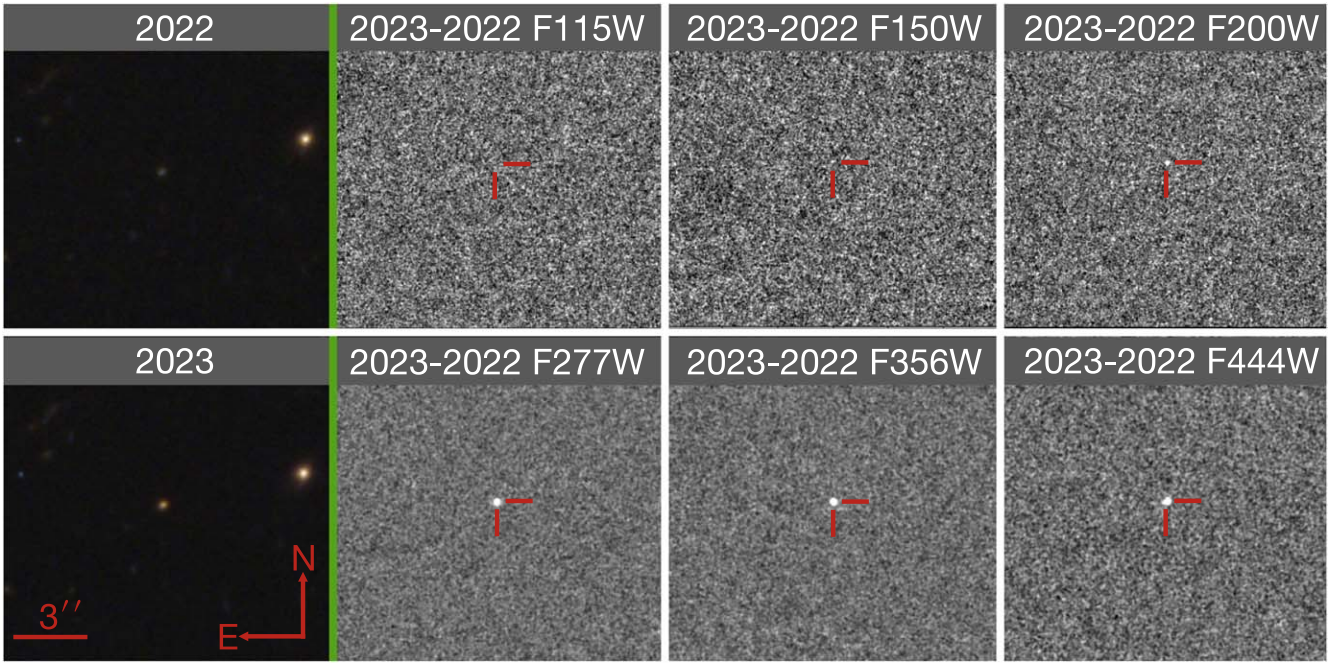


**Figure 1.** (Left column) Full color images using F115W+F150W (blue), F200W+F277W (green), and F356W+F444W (red), with the 2022 JADES epoch on top and 2023 (including SN 2023adsy) on the bottom. (Columns 2–4) Difference images created from the two JADES epochs (2023−2022), with the SN 2023adsy position marked with a red indicator. All images are drizzled to 0.″03/ pix and have the same spatial extent.

1.12.5; Bushouse et al. 2022) with context file jwst_1183.pmap to produce 2D spectral data (Figure 2). The pipeline applied a slit-loss throughput correction for SN 2023adsy based on the planned position of a point-source within the MSA shutters (Figure 2). The spectra of the SN and its host galaxy were extracted using the optimal extraction algorithm from Horne (1986) implemented as scripts available as part of the MOS Optimal Spectral Extraction notebook.[25] We used `webbpsf` to generate the PSF for the NIRSpec observation. As there is no obvious extended emission from the host galaxy, we used a Gaussian kernel to model the flux distribution in the 2D spectrum. The raw Host+SN spectrum is shown in the bottom of Figure 2, used for the spectroscopic redshift measurement, and the final SN spectrum used for classification is shown and analyzed in Figure 3.

## 3. Classification as Type Ia

### 3.1. Spectroscopic Classification

The first step for our classification is to obtain a spectroscopic redshift by identifying host-galaxy emission lines. The two most prominent features are best matched by [O III] and H$\alpha$, which have rest-frame wavelengths of $\sim$5008 Å and $\sim$6565 Å and provide a robust spectroscopic redshift of $z = 2.903 \pm 0.007$ for SN 2023adsy (Figure 2). We use this value for all analysis going forward.

Next, we remove the host-galaxy emission lines from the spectrum and use the Next Generation SuperFit (`NGSF`; Goldwasser et al. 2022)[26] package to classify SN 2023adsy. We note that by removing the H$\alpha$ emission line we could plausibly be removing SN flux if SN 2023adsy were of Type II, but the width of the line is precisely at the resolution of the Prism (i.e., $\sim$3000 km s$^{-1}$). indicating a narrow emission line consistent with low-velocity host emission. We are therefore confident we are removing H$\alpha$ exclusively from the host galaxy, as a contribution from the SN would result in a line width much broader than what is observed (see the comparison to the SN IIP 2016esw in Figure 3). A narrow emission line could be seen from an SN IIn, but the best-fit SN IIn `NGSF` match to the preclipped spectrum (Figure 2) results in $\chi^2/\nu = 2.16$, which is still worse than the SN Ia match (see below). Additionally, SN IIn relative rates are much lower than the SN subtypes we are using for comparison (only $\sim$5% of SNe; Li et al. 2011), making such a discovery very unlikely. Of the top 10 reference SN spectra matched to the SN 2023adsy spectrum, 6 are of Type Ia and the remainder are core-collapse (CC) subtypes, with the best match being Type Ia (Figure 3 and Table 2). The SN Ia spectral template match provides an $\chi^2$ per degree of freedom (DOF; $\nu$) of 1.72, while the next best fit is an SN Ic with 1.92 (all values are given in Table 2). The primary features being matched are the 6150 Å Si II and 8300 Å Ca II absorptions, which are present in the template SN Ia spectrum and SN 2023adsy but either not present (Si II) or not well matched (Ca II) in the CC spectral templates. The Ca II feature is the strongest in the spectrum, with a measured velocity of $\sim$19,000 $\pm$ 2000 km s$^{-1}$ (Figure 4). This is relatively high compared to average low-$z$ SNe Ia, about 1–2$\sigma$ above of the observed distribution (Siebert et al. 2019, 2023), but consistent with a Ca-rich SN (see Section 3.3). Given the phase (relative to peak $B$-band brightness) of the best-fit spectral template for each SN subtype, the inferred observer-frame times of peak $B$-band brightness are given in Table 2 alongside the reduced-$\chi^2$ values and compared to the results from light-curve fitting in Section 3.2.

### 3.2. Photometric Classification

While the spectroscopic template matching from the previous section suggests that SN 2023adsy is indeed an SN Ia

[25] https://spacetelescope.github.io/jdat_notebooks/notebooks/ifu_optimal/ifu_optimal.html
[26] https://github.com/oyaron/NGSF

**Table 1**
Observations for SN 2023adsy Discussed in Section 2

| PID | MJD | Instrument | Filter/Disperser | $m_{AB}$ |
|---|---|---|---|---|
| 1180 | 60220 | NIRCam | F090W | >30.2 |
| 1180 | 60220 | NIRCam | F115W | >30.6 |
| 1180 | 60220 | NIRCam | F150W | $30.39 \pm 0.18$ |
| 1180 | 60221 | NIRCam | F200W | $28.98 \pm 0.09$ |
| 1180 | 60220 | NIRCam | F277W | $28.26 \pm 0.05$ |
| 1180 | 60220 | NIRCam | F335M | $28.00 \pm 0.07$ |
| 1180 | 60220 | NIRCam | F356W | $28.10 \pm 0.06$ |
| 1180 | 60220 | NIRCam | F410M | $28.07 \pm 0.08$ |
| 1180 | 60220 | NIRCam | F444W | $28.06 \pm 0.07$ |
| 1180 | 60264 | NIRCam | F090W | >29.9 |
| 1180 | 60264 | NIRCam | F115W | >30.3 |
| 1180 | 60264 | NIRCam | F150W | >30.1 |
| 1180 | 60264 | NIRCam | F200W | $29.00 \pm 0.12$ |
| 1180 | 60264 | NIRCam | F277W | $28.41 \pm 0.08$ |
| 1180 | 60264 | NIRCam | F335M | $28.13 \pm 0.09$ |
| 1180 | 60264 | NIRCam | F356W | $28.45 \pm 0.09$ |
| 1180 | 60264 | NIRCam | F410M | $28.57 \pm 0.17$ |
| 1180 | 60264 | NIRCam | F444W | $28.21 \pm 0.11$ |
| 6541 | 60276 | NIRCam | F115W | >28.9 |
| 6541 | 60276 | NIRCam | F150W | >29.6 |
| 6541 | 60276 | NIRCam | F200W | $28.86 \pm 0.18$ |
| 6541 | 60276 | NIRCam | F277W | $28.53 \pm 0.15$ |
| 6541 | 60276 | NIRCam | F356W | $28.49 \pm 0.16$ |
| 6541 | 60276 | NIRCam | F444W | $28.67 \pm 0.29$ |
| 1180 | 60311 | NIRCam | F090W | >29.4 |
| 1180 | 60311 | NIRCam | F115W | >29.9 |
| 6541 | 60310 | NIRCam | F150W | >29.9 |
| 6541 | 60310 | NIRCam | F200W | $29.33 \pm 0.19$ |
| 6541 | 60310 | NIRCam | F277W | $28.46 \pm 0.15$ |
| 1180 | 60311 | NIRCam | F335M | $28.26 \pm 0.10$ |
| 6541 | 60310 | NIRCam | F356W | $28.47 \pm 0.17$ |
| 1180 | 60311 | NIRCam | F410M | >28.4 |
| 6541 | 60310 | NIRCam | F444W | >28.9 |
| 6541 | 60310 | NIRSpec | Prism | ⋯ |

**Note.** Columns are JWST Program ID, Modified Julian date, JWST instrument, filter or grating, and photometry plus final uncertainty for SN 2023adsy. Upper limits are $2\sigma$.

with a best-fit $\chi^2/\nu = 1.72$, there is still a possibility that SN 2023adsy is a CC SN given the spectrum alone, as all best-fit CC SN spectral matches, has a reasonable $1.92 < \chi^2/\nu < 2.5$. We fit the measured photometry with the SALT3-NIR SN Ia light-curve model (Pierel et al. 2022; see Section 4.1) and all existing CC SN light-curve evolution models with rest-frame optical to near-IR (to observer-frame $\sim 4\,\mu$m) wavelength coverage (Pierel et al. 2018). We include Galactic dust based on the maps of Schlafly & Finkbeiner (2011) and the reddening law from Fitzpatrick (1999), which corresponds to $E(B-V) = 0.01$ mag with $R_V = 3.1$. We also allow for a large amount (up to $E(B-V) = 1.5$ with $1 < R_V < 5$) of rest-frame, host-galaxy dust in the CC SN light-curve fits and a SALT3-NIR color parameter range of $-1.5 < c < 1.5$ given the very red observed colors.

Figures 5 and 6 show the best-fit models for each SN subtype in all filters. The resulting reduced $\chi^2$ and measured time of peak $B$-band brightness for each model are shown in Table 2 alongside the results from the spectroscopic analysis in Section 3.1. The SN Ib and SN Ic subtypes are heavily disfavored (best-fit $\chi^2/\nu = 4.86$ and 6.00, respectively) compared to SN Ia ($\chi^2/\nu = 0.95$). The SN IIP model is a reasonable fit to the data ($\chi^2/\nu = 1.34$), but the measured time of peak $B$-band brightness is $26\sigma$ lower than that inferred by spectral template matching (Table 2). This corresponds to a difference between light-curve and spectral fits of $\sim$20 rest-frame days, while the SN Ia time of peak measurements from the light curve and spectrum agree within $2\sigma$ ($\sim$1 rest-frame day). Therefore the spectroscopic and photometric classification work give consistent results only for SN Ia, both suggesting that we are seeing an SN Ia evolving from $\sim -5$ to $+20$ rest-frame days relative to peak brightness with the spectrum taken at the end of this range (Tables 1 and 2). We also note that the CC SN $\chi^2/\nu$ values in Table 2 are from the best-fit models, while the distributions for all templates for SN Ib, SN Ic, and SN IIP are $5.82 \pm 0.66$, $7.43 \pm 0.39$, and $3.78 \pm 0.43$, respectively. Finally, the $E(B-V)$ reddening values measured for these best-fit templates (with $R_V = 3.1$) are 0.01, 0.30, and 0.42 respectively. Apart from the SN Ib model, which was the worst fit to the data, these are also fairly high values, indicating that SN 2023adsy is indeed a particularly red object.

Finally, we turn to the rest-frame near-infrared (near-IR) photometry, where SNe Ia have a distinct second maximum that should differentiate the SN subclasses (e.g., Mandel et al. 2022; Pierel et al. 2022). Figure 7 shows the observed rest-frame near-IR colors versus rest-frame near-IR magnitude for SN 2023adsy compared to the best-fit SN Ia and CC SN models. We restrict the comparison to rest-frame rzY filters, where the light-curve models are most robust. The evolution in rest-frame near-IR color–magnitude space is well matched by the SN Ia template, while the CC SN templates fail to reproduce the observed trends as accurately. The SN Ic and SN IIP models are the next best matches in color–magnitude space, but SN Ic is ruled out by the overall much poorer light-curve fit ($\chi^2/\nu = 7.20$) and SN IIP by the combination of poor spectral match ($\chi^2/\nu = 2.24$) and large discrepancy between time of peak $B$-band brightness inferred from light-curve and spectral fitting. We therefore conclude that the combination of imaging and spectroscopy for SN 2023adsy is sufficient to classify SN 2023adsy as a likely SN Ia at $z = 2.903$.

### 3.3. Comparison to low-z Ca-rich SNe Ia

Using the full wavelength range of the spectrum, the best-match spectral template for SN 2023adsy from NGSF is a normal SN Ia despite the presence Ca-rich templates in the database. We turn to the population of Ca-rich SNe Ia to explain the high observed Ca II velocity and red color (i.e., high value of $c$) but note that SN 2023adsy appears to best match a normal SN Ia apart from these characteristics. We find that the Ca II velocity ($\sim$18,000 km s$^{-1}$) and red intrinsic color ($c \sim 1$ near peak brightness) of SN 2016hnk, both measured by Galbany et al. (2019) and Jacobson-Galán et al. (2020), are the best match to SN 2023adsy ($\sim$19,000 km s$^{-1}$ and $c \sim 0.9$). We show a comparison of SN 2016hnk at $\sim$10 days after peak brightness to the SN 2023adsy spectrum in Figure 3 and focus on the Ca II feature in Figure 4. The match is quite good despite NGSF preferring a normal SN Ia, suggesting that SN 2023adsy may share some properties with Ca-rich transients (both observed and theoretical; Woosley et al. 1986; Bildsten et al. 2007; Perets et al. 2010; Shen et al. 2010; Waldman et al. 2011; Kasliwal et al. 2012; Foley 2015; De et al. 2020; Zenati et al. 2023). We note that while the color at peak $B$-band brightness

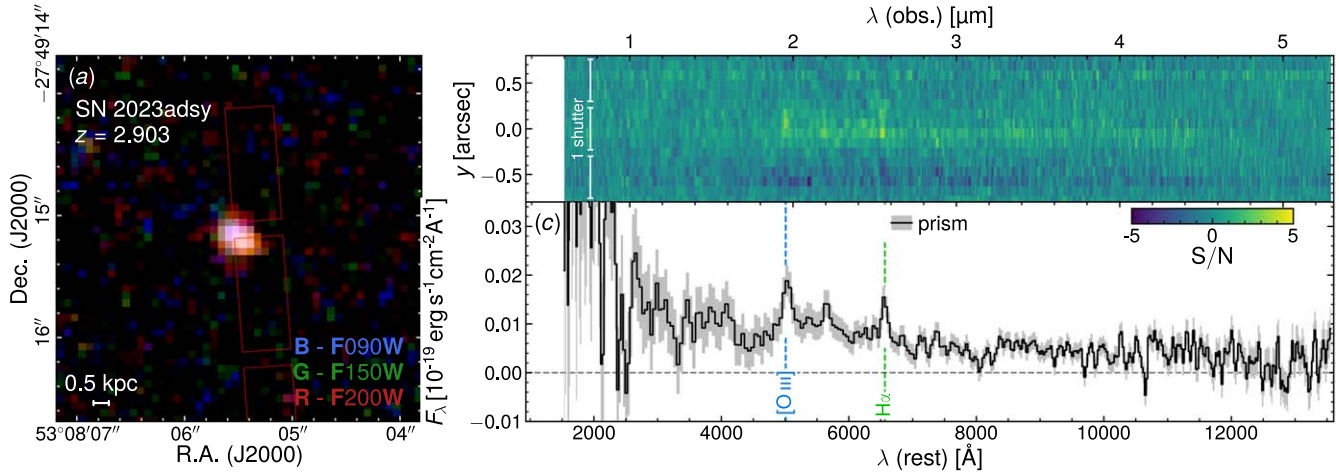


**Figure 2.** (a) The slitlet positions over SN 2023adsy for one of the dithered observations. The reported slitlet position (shown) is slightly offset from its true position, which we confirm contains the SN. (b)/(c) The 2D- and 1D-extracted NIRSpec spectrum for SN 2023adsy. The primary host emission lines ([O III] and H$\alpha$) used for the spectroscopic redshift measurement are shown with dotted lines.

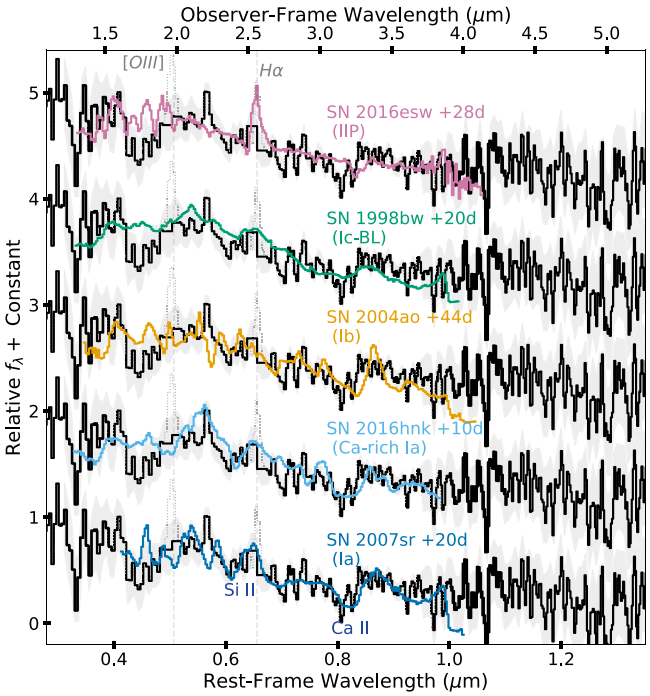


**Figure 3.** The observed NIRSpec spectrum (with uncertainty) of SN 2023adsy is shown as a black solid line, with the primary features used for the preferred SN Ia classification labeled (bottom). The observed host-galaxy emission lines (faint dotted lines) are marked and have been removed from the spectrum, with a redshift of $z = 2.903$ applied. The best-match template from NGSF is a SN Ia (blue, bottom), and a Ca-rich SN Ia subclass is also shown for comparison. The best CC matches are also shown, including Ib (red, third from bottom), Ic (pink, second from top), and IIP (light blue, top). While SN Ia is favored based on the spectrum, we also use the photometry and host-galaxy information to make the final classification.

and Ca II velocity seem to match well between these two objects, the absolute $B$-band magnitude of SN 2023adsy is $\sim$1 mag brighter than SN 2016hnk before standardization ($M_B \sim -16.5$ assuming $\Lambda$CDM). This puts SN 2023adsy more in the luminosity range of 91bg-like SNe Ia (Filippenko et al. 1992; Taubenberger et al. 2008; Sullivan et al. 2011; Taubenberger 2017), but unlike the fast-declining 91bg-like SNe Ia our fits to SN 2023adsy are consistent with a normal decline rate (see Section 4.1). More SNe Ia in this new redshift range are needed to determine if SN 2023adsy is peculiar, or if very high-$z$ SNe Ia typically share properties with both normal and less common SN Ia subtypes.

**Table 2**
The Time of Peak $B$-band Brightness ($t_{pk}$) Inferred from the Light-curve Fitting Compared to the Best Spectral Template Match for Each SN Type, as well as the Reduced $\chi^2$ ($\chi^2/\nu$) for Each Method

| SN Type | Light Curve | | Spectroscopic | |
|---|---|---|---|---|
| | $t_{pk}$ | $\chi^2/\nu$ | $t_{pk}$ | $\chi^2/\nu$ |
| Ia | $60240 \pm 2$ | 0.95 | 60236 | 1.72 |
| Ib | $60127 \pm 4$ | 4.86 | 60138 | 2.47 |
| Ic | $60120 \pm 4$ | 6.00 | 60232 | 1.92 |
| IIP | $60123 \pm 3$ | 1.34 | 60201 | 2.24 |

**Note.** Columns are SN-type model/spectral template used, the time in Modified Julian Date of peak $B$-band brightness measured from light-curve fitting (to the data <4 $\mu$m where models are better constrained), the light-curve fitting $\chi^2$ per DOF ($\nu$) without model uncertainties, as they do not exist for CC SN models, the time of peak $B$-band brightness given the best-fit spectroscopic template match, and the $\chi^2$ per DOF of the best-fit spectroscopic template match.

## 4. Luminosity Distance Measurement

### 4.1. Light-curve Fitting

We begin by fitting the observed photometry (including upper limits; Table 1) with the SALT3-NIR SN Ia light-curve evolution model (Pierel et al. 2022), which has a rest-frame wavelength coverage of $\sim$2500–20,000Å. In addition to the basic light-curve parameters of redshift, amplitude ($x_0$), and time of peak brightness ($t_{pk}$), SALT3-NIR parameterizes SN Ia light curves with the "shape" or "stretch" ($x_1$) and color ($c$) parameters. These are used in Section 4.3 to make the traditional corrections to the observed peak apparent magnitude needed to obtain a standardized luminosity distance (e.g., Tripp 1998). We include the same 0.01 mag Galactic extinction correction as in Section 3.2 and allow for high values for the SALT3-NIR color parameter (up to $c = 1.5$). For this stage, it is critical that the measured $x_1$ and $c$ values are accurate, but including the poorly constrained SALT3-NIR rest-frame

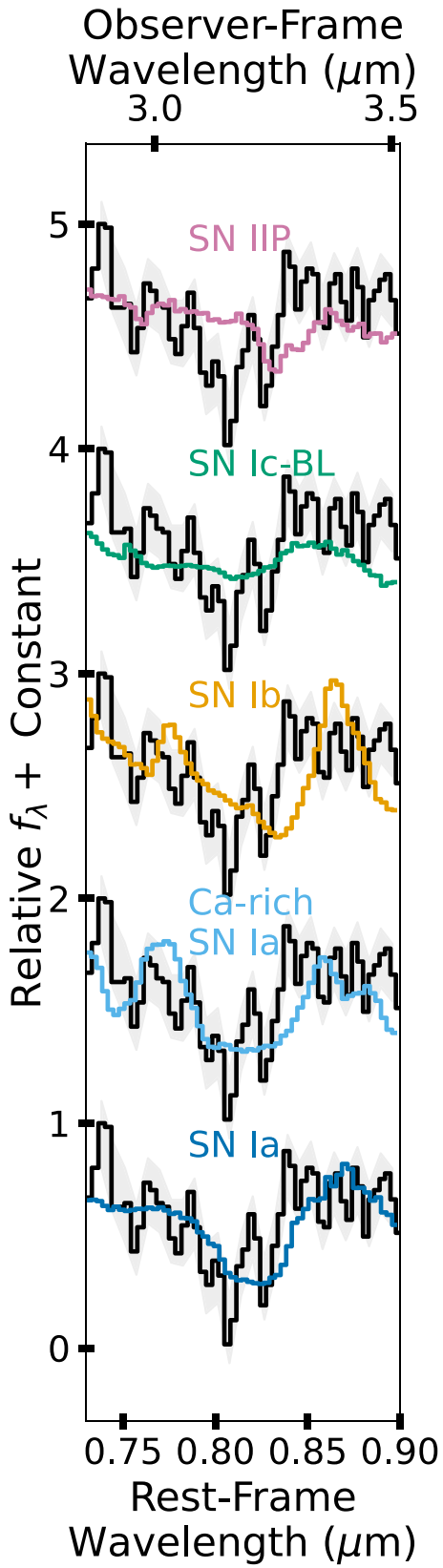


**Figure 4.** The same as Figure 3 but zoomed in on the Ca II feature, where the SN Ia and Ca-rich subclass are the best fit.

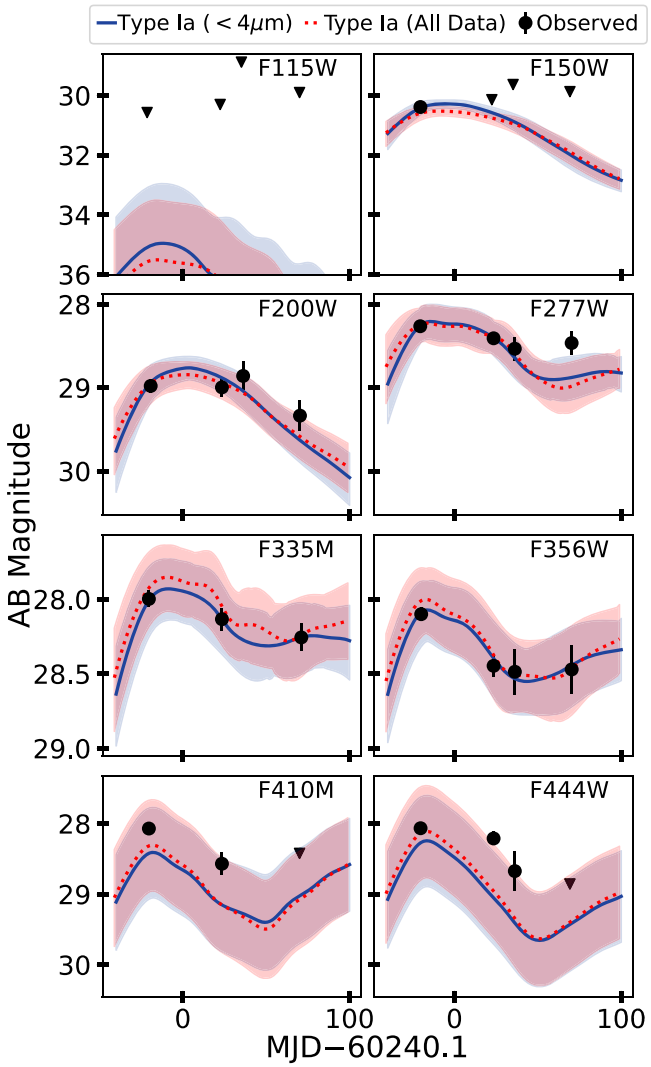


**Figure 5.** The photometry measured in Section 2.1 is shown as black circles with error, with ($5\sigma$) upper limits denoted by triangles. The fit to the full light curve is shown in red (dashed, with error), and the fit to data <4 $\mu$m (i.e., without F410M and F444W) is shown in blue (solid, with error). While the resulting model prediction for the >4 $\mu$m data remains roughly the same, the model at <4 $\mu$m becomes biased as it attempts to vary the parameters extremely to better fit the reddest data. While the fits are of similar quality, we use the fit to the <4 $\mu$m data for our distance modulus measurement as all filters are well fit without resulting in extreme parameter values (Section 4.1).

$J$-band leads to biased parameters when included in the fit (red model; Figure 5). We therefore remove the F410M and F444W filters from the fit for an accurate standardization, resulting in the blue model in Figure 5. The bounds and retrieved SALT3-NIR parameters from the fit are shown in Table 3.

The best-fit model is shown with the observed photometry in Figure 5. SALT3-NIR is an excellent fit in all filters below 4 $\mu$m and matches the $F410M/F444W$ filters within $1\sigma$ but is systematically fainter than these reddest filters whether they are included in the fit or not. This could be due to the large uncertainties in the rest-frame $J$-band model (Pierel et al. 2022), an issue with the PSF model used at these reddest wavelengths, and/or a zero-point offset in the 4 $\mu$m data. We note that the $F410M/F444W$ fit improves (without a change to the $c$ parameter) when the near-IR SALT3-NIR color law is replaced with the dust law from Fitzpatrick (1999). The SALT3-NIR color law is predicted to trace a dust law in the near-IR but currently diverges slightly (Pierel et al. 2018, 2022). A larger sample of near-IR SN Ia observations is needed to determine if an improved color law would resolve the poor fit to the 4 $\mu$m

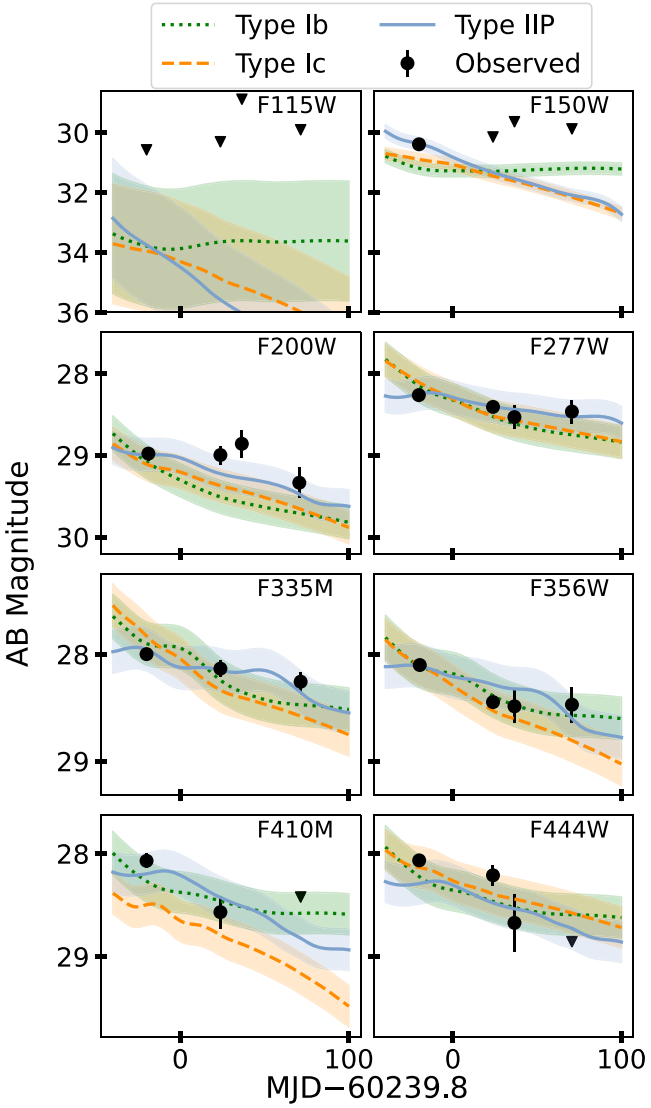


**Figure 6.** The photometry measured in Section 2.1 is shown as black circles with error, with ($5\sigma$) upper limits denoted by triangles. The best-fit SN Ib (green dotted line), SN Ic (orange dashed line), and SN IIP (blue solid line) models are shown for comparison. Unlike SALT3-NIR these spectral templates do not have a defined model covariance, and so the uncertainties are purely statistical.

data, but this result indicates the color law is a possible culprit. Regardless, when the 4 $\mu$m data are included, the fitter attempts to vary the model parameters to an extreme degree in order to improve the fit, biasing the results. Since the resulting fit is not a large improvement in the $>4$ $\mu$m filters and degrades the fit at $<4$ $\mu$m, we proceed with the fit to data with wavelengths $<4$ $\mu$m (rest-frame $\leqslant 1$ $\mu$m).

### 4.2. Simulations for Bias Correction

We simulate SN 2023adsy observations from the discovery JADES epoch using the Supernova Analysis (SNANA) code (Kessler et al. 2009, 2019) to make an approximate correction for bias from selection effects, Malmquist bias, and light-curve fitting bias from our luminosity distance measurement for SN 2023adsy. SNANA simulates SN light curves for an arbitrary set of survey properties while accounting for variations in noise, PSF, and cadence. Due to its speed, accuracy, and flexibility, SNANA has become the standard tool for simulating SN surveys in recent years (e.g., Betoule et al. 2014; Scolnic et al. 2018; Jones et al. 2019; Kessler et al. 2019; Rose et al. 2021b; Brout et al. 2022). Following Figure 1 in Kessler et al. (2019), a brief overview of the SNANA simulation scheme that we apply to this analysis is as follows:

1. *Source Model*
   (a) Generate the source spectral energy distribution (SED) at each simulated epoch using SALT3-NIR. We use SN Ia parameter distributions from Popovic et al. (2023) but extend the color range out to $c = 1.1$ to match the particularly red color of this SN.
   (b) Apply cosmological dimming, Galactic extinction, weak lensing, and redshift to the SED. We simulate every SN at the SN 2023adsy redshift of 2.903 as there is negligible uncertainty in the redshift.
   (c) Integrate the redshifted SED over each filter transmission function to create the noise-free photometric light curve.
2. *Noise Model*
   (a) Use image zero point to convert each true light curve in magnitude to true flux in photoelectrons.
   (b) Compute flux uncertainty from zero point, PSF, and sky noise, which are determined on a per-epoch basis from the real JADES observations. These uncertainties are used to apply Gaussian random fluctuations to true fluxes.
3. *Trigger Model*
   (a) Check for detection (S/N $>3\,\sigma$ in two or more bands).
   (b) Write selected events in data files.

We simulate a sample of 20,000 SNe Ia and fit the full sample with SALT3-NIR. After fitting, we then select the SN sample that has best-fit parameters that closely match the real best-fit parameters $x_1$ and $c$. We assume the true $\alpha$ and $\beta$ are equal to those measured by the Pantheon+ team (Brout et al. 2022), as discussed in Section 4.3. The $\alpha$ and $\beta$ values were estimated from a large SN sample, and therefore their uncertainties should have a negligible impact on the uncertainties for a single SN (though $z$-dependent evolution in these parameters is a potential concern that we do not address in this work). For that simulated set, the bias correction is the average difference between the Tripp-derived distance modulus when the fitted parameters are used versus the Tripp-derived distance modulus when the simulated parameters are used.

This method is an approximation of the BEAMS with Bias Corrections (BBC) method (Kunz et al. 2007, 2013; Kessler & Scolnic 2017), which estimates a correction term $\Delta\mu_{\rm Bias}$ from the difference between simulated versus recovered parameters based on a large simulated sample of SNe Ia in a 5D space of $\{z, x_1, c, \alpha, \beta\}$ (see Section 4.3).

The methods follow those of previous cosmological analyses (e.g., Scolnic et al. 2018) with the modest simplifications described above due to having just a single SN instead of hundreds to thousands.

From this approach, we find that the bias correction is fairly negligible at $\sim$2%, though we still include it in the final luminosity distance measurement (Section 4.3). This implies that nearly all normal SNe Ia within the observed range of $x_1$, $c$ values would be detected by our survey at this redshift, due to the extreme-depth excellent wavelength coverage provided by the JADES program (Table 1).

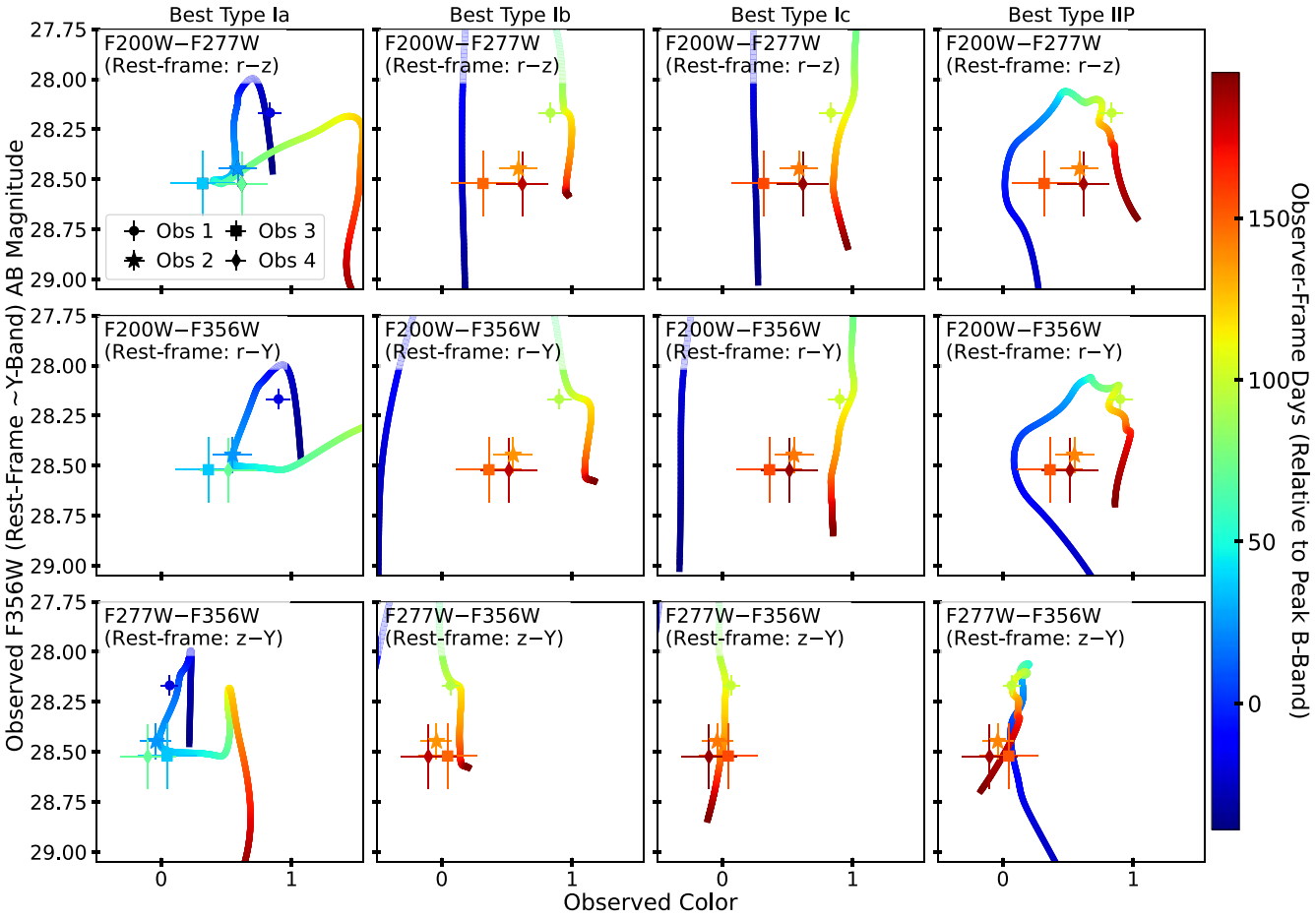


**Figure 7.** Three observed colors (labeled by row) vs. magnitude (F356W; rest-frame $\sim Y$-band) shown as black points with error bars, with the symbols corresponding to the four observed epochs (legend in upper-left; order of observations is circle, star, square, diamond). The colored lines track the corresponding color–magnitude space as a function of time from best-fit models, with SN Ia in the left column (see Section 4.1) and the top three CC SN model fits in the remaining columns. The coloring of the lines is described by the color bar (right), with early times shown as blue and late times as red. The SN Ia model is the only one to accurately represent the observed color–magnitude relationships in the near-IR as a function of time.

**Table 3**
The SALT3-NIR Light-curve Model Parameters used in This Analysis

| Parameter | Bounds | Best Fit |
|---|---|---|
| $z$ | Fixed | $z = 2.903$ |
| $t_{\rm pk}$ | [60200, 60320] | $60239.98^{+1.50}_{-1.70}$ |
| $x_0$ | [0, 1] | $(7.12^{+0.66}_{-0.55}) \times 10^{-9}$ |
| $x_1$ | [−3, 3] | $-0.11^{+1.03}_{-1.06}$ |
| $c$ | [−1.5, 1.5] | $0.92^{+0.04}_{-0.05}$ |

### 4.3. Extending the Hubble Diagram to z = 3

We transform fitted SALT3-NIR light-curve parameters from Section 4.1 into a distance by way of a modified Tripp formula (Tripp 1998):

$$\mu = m_B - M + \alpha x_1 - \beta c + \delta_{\rm host} + \Delta\mu_{\rm Bias}, \quad (1)$$

where $\mu$ is the distance modulus, $m_B$ is the peak apparent magnitude in the rest-frame $B$ band, $\alpha$ ($\beta$) is the coefficient of relation between SN Ia luminosity and stretch (color), and $M$ is the peak absolute magnitude of an $x_1 = c = 0$ SN Ia assuming some nominal value of $H_0$ (here $H_0 = 70\,{\rm km\,s^{-1}\,Mpc^{-1}}$ and $M = -19.36$). The $\delta_{\rm host}$ parameter is the host-galaxy mass step, or the small residual correlation between SN Ia distance measurements and their host-galaxy masses (Kelly et al. 2010; Lampeitl et al. 2010; Sullivan et al. 2010); because the nature and evolution of the host-galaxy mass step is unknown, especially at such high redshift (e.g., Childress et al. 2014), we simply apply half of the host mass step (for a low-mass galaxy; see Section 5) from Brout et al. (2022; they found $\sim$0.054 mag using the same scatter model implemented in Section 4.2) and add a systematic error of half the host mass step in quadrature. Finally, the $\Delta\mu_{\rm Bias}$ term is a selection bias correction determined by BBC, described in Section 4.2, which we constrain to be $-0.018$ mag for this analysis. Without a large sample of high-$z$ SNe to measure the nuisance parameters ($\alpha$, $\beta$), we fix $\alpha = 0.148$ and $\beta = 3.09$ (these parameters do not seem to change with redshift, but more high-$z$ SNe Ia are needed to confirm the result; Scolnic et al. 2018), which are the best constraints from $z \lesssim 2$ SNe Ia by Brout et al. (2022). The $m_B$ parameter found by the SALT3-NIR model to be 30.73, and the shape/color parameters are shown in Table 3.

The final luminosity distance measurement is $47.18^{+0.27}_{-0.28}$ mag, while the $\Lambda$CDM prediction at $z = 2.903$ (with $H_0 = 70\,{\rm km\,s^{-1}\,Mpc^{-1}}$) is $\mu = 46.91$ mag, a $\lesssim 1\sigma$ difference (Figure 8). The uncertainty on $\mu$ includes the fitted model uncertainties, errors from redshift and peculiar velocity (which are

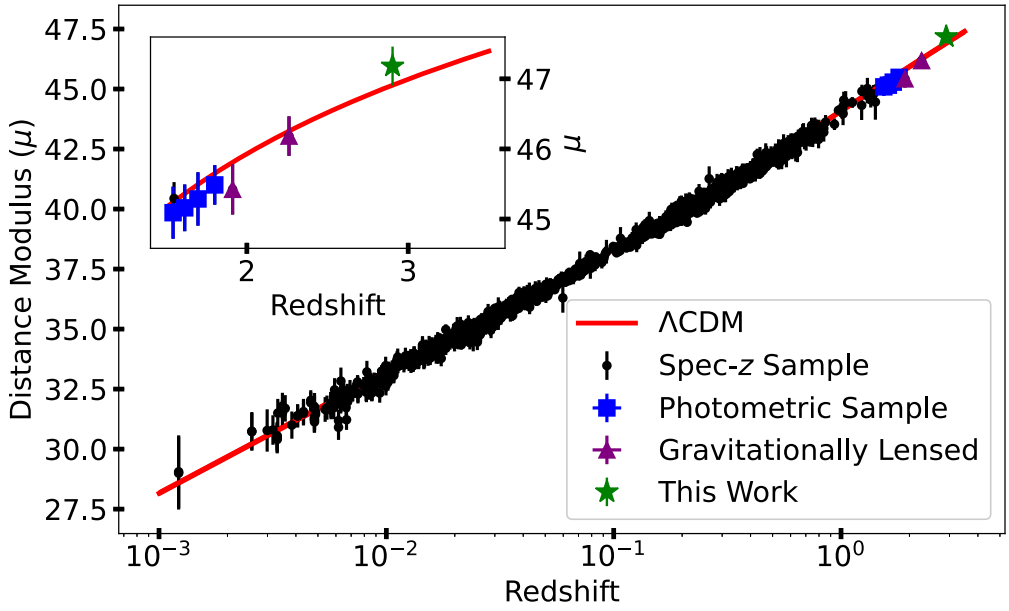


**Figure 8.** Luminosity distance measurements from the full sample of SNe Ia from Brout et al. (2022) extending to $z = 2.22$. Black points (with errors) are SNe Ia with spectroscopic classifications, while blue squares (with error) are SNe Ia with photometric classifications. The two gravitationally lensed SNe Ia with distance measurements are shown as purple triangles. SN 2023adsy is shown as a green star, and ΛCDM is shown as a solid red line for reference. The width of the red line encompasses the width of the current $H_0$ tension, with the center of the line used for reference.

negligible here), the intrinsic scatter of SNe Ia (0.1 mag; Scolnic et al. 2018), and an additional $0.005z$ mag uncertainty from weak gravitational lensing (Jönsson et al. 2010). We note that SN 2023adsy would not pass fiducial cosmological cuts ($|c| < 0.3$; Scolnic et al. 2018) because of its red color ($c \sim 0.9$), but the color correction for SN Ia standardization has been shown to hold to very high values of $c$ (∼0.8) across large samples (Rose et al. 2021a; Ginolin et al. 2024). Therefore we apply the traditional standardization, which nevertheless results in this agreement with ΛCDM. More high-$z$ SNe Ia are required to determine if there is true drift in the normal SN Ia population parameters, meaning high-$z$ SNe Ia could be intrinsically redder than low-$z$ SNe Ia while still adhering to a normal Tripp equation for standardization, or if this object is peculiar for its redshift.

## 5. Discussion

We have presented JWST observations of an SN (SN 2023adsy) with a spectroscopic redshift of $z = 2.903 \pm 0.007$, which we classify using both the spectrum and light-curve information as the most distant SN Ia yet discovered. We note that SN 2023adsy could plausibly still be a CC SN that appears different from our finite low-$z$ library of spectra and light-curve models, but a larger sample of high-$z$ CC Se observed a light curve with a model for SN Ia evolution that includes a traditional shape and color parameterization and uses our current best understanding of SN Ia standardization at lower redshift ($z \lesssim 2$) to measure the luminosity distance to SN 2023adsy. Although SN 2023adsy would not pass fiducial low-$z$ cosmology cuts because of its red color, we find a value of $\mu = 47.18^{+0.27}_{-0.28}$ mag including a correction for potential observational biases, which is in excellent agreement ($\lesssim 1\sigma$) with ΛCDM. Although a single object is not enough to directly constrain cosmological parameters at high $z$, any significant deviation of SN Ia luminosity distances from ΛCDM at $z > 2$ would be a strong indicator of SN Ia luminosity evolution with redshift. The agreement of SN 2023adsy with ΛCDM, the most distant such test, gives no indication of significant SN Ia luminosity evolution with redshift.

Despite agreement between the SN 2023adsy luminosity distance measurement and standard cosmology, there are two observed peculiarities with SN 2023adsy. The first is its very red observed color ($c \sim 0.9$), and the second is its high Ca II velocity (∼19000 km$^{-1}$). The red color could be attributed to significant dust attenuation from the host galaxy JADES-GS +53.13485−27.82088,[27] but fitting photometry of the host galaxy from 2022 (well before the SN explosion; Eisenstein et al. 2023) with the Bayesian Analysis of Galaxies for Physical Inference and Parameter EStimation (Carnall et al. 2018) infers a fairly low-mass ($\sim 10^8 M_\odot$), low-metallicity ($\sim 0.3 Z_\odot$), low-extinction ($A_V < 0.1$) host galaxy, suggesting that SN 2023adsy could be intrinsically red. However, measurements of SN 2023adsy's local environment could change this interpretation. At this distance intergalactic reddening could also be a factor but is unlikely to contribute more than ∼0.15 mag at $z = 2.903$ (Ménard et al. 2008). Low-$z$ SNe with high Ca II velocities tend to be redder than the general population of SNe Ia (Siebert et al. 2019), but SN 2023adsy is still fairly extreme in both parameters. The low-$z$ SN 2016hnk is a good match to both the SN 2023adsy color and Ca II velocity but has a ∼1 mag fainter absolute magnitude before standardization. SN 2023adsy has an absolute magnitude closer to 91bg-like SNe Ia but with a normal light-curve decline rate. We require a larger population of high-$z$ SNe Ia to determine if SN 2023adsy is truly an outlier that should be cut from future cosmological constraints (i.e., most normal high-$z$ SNe Ia fall within traditional low-$z$ cosmology cuts) or if the distribution of SN Ia properties varies significantly with redshift due to changes in progenitors or their environment.

SN 2023adsy is the first SN Ia candidate with a combined spectroscopic and photometric data set in the dark matter-dominated universe at $z > 2$, making this the first robust test for

[27] JADES Host ID 96906 from https://archive.stsci.edu/hlsp/jades.

SN Ia standardized luminosity evolution in the manner suggested by Riess & Livio (2006). JWST is the only resource capable of expanding this sample further and is expected to do so with $\gtrsim$10 additional such objects anticipated over the next 2 years (Pierel et al. 2024a). While SN 2023adsy gives no indication that standardized SN Ia luminosities evolve significantly with redshift, the full sample will be required to confirm this result and put constraints on any possible evolution at lower redshift for future cosmological measurements.

## Acknowledgments

We would like to thank Erin Hayes, Saurabh Jha, and Rick Kessler for the useful discussion. We thank the DDT and JWST/HST scheduling teams at STScI for the extraordinary effort in getting the DDT observations used here scheduled quickly. This work is based on observations made with the NASA/ESA/CSA James Webb Space Telescope. The data were obtained from the Mikulski Archive for Space Telescopes at the Space Telescope Science Institute, which is operated by the Association of Universities for Research in Astronomy, Inc., under NASA contract NAS 5-03127 for JWST. These observations are associated with program #1180 and 6541. Part of the JWST data used in this Letter can be found in MAST (Rieke et al. 2023; JADES DR1). Additionally, this work made use of the *lux* supercomputer at UC Santa Cruz, which is funded by NSF MRI grant AST 1828315, as well as the High Performance Computing (HPC) resources at the University of Arizona, which is funded by the Office of Research Discovery and Innovation (ORDI), Chief Information Officer (CIO), and University Information Technology Services (UITS). A.J.B. acknowledges funding from the "First-Galaxies" Advanced Grant from the European Research Council (ERC) under the European Union's Horizon 2020 research and innovation program (grant agreement No. 789056). P.A.C., E.E., D.J.E., and B.D.J. are supported by a JWST/NIRCam contract to the University of Arizona, NAS5-02015. D.J.E. is also supported as a Simons Investigator. R.M. acknowledges support by the Science and Technology Facilities Council (STFC), by the ERC through Advanced Grant 695671 "QUENCH," and by the UKRI Frontier Research grant RISEandFALL. R.M. also acknowledges funding from a research professorship from the Royal Society. B.E.R. acknowledges support from the NIRCam Science Team contract to the University of Arizona, NAS5-02015, and JWST Program 3215. JDRP is supported by NASA through a Einstein Fellowship grant No. HF2-51541.001 awarded by the Space Telescope Science Institute (STScI), which is operated by the Association of Universities for Research in Astronomy, Inc., for NASA, under contract NAS5-26555.

## ORCID iDs

J. D. R. Pierel https://orcid.org/0000-0002-2361-7201
M. Engesser https://orcid.org/0000-0003-0209-674X
D. A. Coulter https://orcid.org/0000-0003-4263-2228
C. DeCoursey https://orcid.org/0000-0002-4781-9078
M. R. Siebert https://orcid.org/0000-0003-2445-3891
A. Rest https://orcid.org/0000-0002-4410-5387
E. Egami https://orcid.org/0000-0003-1344-9475
W. Chen https://orcid.org/0000-0003-1060-0723
O. D. Fox https://orcid.org/0000-0003-2238-1572
D. O. Jones https://orcid.org/0000-0002-6230-0151
B. A. Joshi https://orcid.org/0000-0002-7593-8584
T. J. Moriya https://orcid.org/0000-0003-1169-1954
Y. Zenati https://orcid.org/0000-0002-0632-8897
A. J. Bunker https://orcid.org/0000-0002-8651-9879
P. A. Cargile https://orcid.org/0000-0002-1617-8917
M. Curti https://orcid.org/0000-0002-2678-2560
D. J. Eisenstein https://orcid.org/0000-0002-2929-3121
S. Gezari https://orcid.org/0000-0003-3703-5154
S. Gomez https://orcid.org/0000-0001-6395-6702
M. Guolo https://orcid.org/0000-0002-5063-0751
B. D. Johnson https://orcid.org/0000-0002-9280-7594
M. Karmen https://orcid.org/0000-0003-2495-8670
R. Maiolino https://orcid.org/0000-0002-4985-3819
R. M. Quimby https://orcid.org/0000-0001-9171-5236
B. Robertson https://orcid.org/0000-0002-4271-0364
M. Shahbandeh https://orcid.org/0000-0002-9301-5302
L. G. Strolger https://orcid.org/0000-0002-7756-4440
F. Sun https://orcid.org/0000-0002-4622-6617
Q. Wang https://orcid.org/0000-0001-5233-6989
T. Wevers https://orcid.org/0000-0002-4043-9400

## References

Becker, A. 2015, HOTPANTS: High Order Transform of PSF ANd Template Subtraction, Astrophysics Source Code Library, ascl:1504.004
Betoule, M., Kessler, R., Guy, J., et al. 2014, A&A, 568, A22
Bildsten, L., Shen, K. J., Weinberg, N. N., & Nelemans, G. 2007, ApJL, 662, L95
Brout, D., Scolnic, D., Popovic, B., et al. 2022, ApJ, 938, 110
Bushouse, H., Eisenhamer, J., Dencheva, N., et al. 2022, JWST Calibration Pipeline, v1.12.5, Zenodo, doi:10.5281/zenodo.7325378
Carnall, A. C., McLure, R. J., Dunlop, J. S., & Davé, R. 2018, MNRAS, 480, 4379
Chen, W., Kelly, P. L., Frye, B. L., et al. 2024, ApJ, 970, 102
Childress, M. J., Wolf, C., & Zahid, H. J. 2014, MNRAS, 445, 1898
De, K., Kasliwal, M. M., Tzanidakis, A., et al. 2020, ApJ, 905, 58
DeCoursey, C., Egami, E., Pierel, J. D. R., et al. 2024, arXiv:2406.05060
DeCoursey, C., Egami, E., Rieke, M., et al. 2023b, TNSAN, 164, 1
DeCoursey, C., Egami, E., Sun, F. & Jades Collaboration 2023a, AAS Meeting Abstracts, 55, 206.03
DeCoursey, C., Sun, F., Egami, E., et al. 2023c, TNSAN, 275, 1
Egami, E., Bonaventura, N., Charlot, S., et al. 2023, JWST Proposal. Cycle 2, ID. #6541
Eisenstein, D. J., Johnson, B. D., Robertson, B., et al. 2023, arXiv:2310.12340
Engesser, M., Brammer, G., Gould, K., et al. 2022b, TNSAN, 145, 1
Engesser, M., Smith, K., Chen, T., et al. 2022a, TNSAN, 155, 1
Ferruit, P., Jakobsen, P., Giardino, G., et al. 2022, åp, 661, A81
Filippenko, A. V. 1997, ARA&A, 35, 309
Filippenko, A. V., Richmond, M. W., Branch, D., et al. 1992, AJ, 104, 1543
Fitzpatrick, E. L. 1999, PASP, 111, 63
Foley, R. J. 2015, MNRAS, 452, 2463
Frye, B. L., Pascale, M., Pierel, J., et al. 2024, ApJ, 961, 171
Galbany, L., Ashall, C., Höflich, P., et al. 2019, åp, 630, A76
Ginolin, M., Rigault, M., Copin, Y., et al. 2024, arXiv:2406.02072
Goldwasser, S., Yaron, O., Sass, A., et al. 2022, TNSAN, 191, 1
Horne, K. 1986, PASP, 98, 609
Jacobson-Galán, W. V., Polin, A., Foley, R. J., et al. 2020, ApJ, 896, 165
Jakobsen, P., Ferruit, P., Alves de Oliveira, C., et al. 2022, A&A, 661, A80
Jones, D. O., Rodney, S. A., Riess, A. G., et al. 2013, ApJ, 768, 166
Jones, D. O., Scolnic, D. M., Foley, R. J., et al. 2019, ApJ, 881, 19
Jönsson, J., Sullivan, M., Hook, I., et al. 2010, MNRAS, 405, 535
Kasliwal, M. M., Kulkarni, S. R., Gal-Yam, A., et al. 2012, ApJ, 755, 161
Kelly, P. L., Hicken, M., Burke, D. L., Mandel, K. S., & Kirshner, R. P. 2010, ApJ, 715, 743
Kessler, R., Bernstein, J. P., Cinabro, D., et al. 2009, PASP, 121, 1028
Kessler, R., Brout, D., D'Andrea, C. B., et al. 2019, MNRAS, 485, 1171
Kessler, R., & Scolnic, D. 2017, ApJ, 836, 56
Kunz, M., Bassett, B. A., & Hlozek, R. A. 2007, PhRvD, 75, 103508
Kunz, M., Hlozek, R., Bassett, B. A., et al. 2013, Astrostatistical Challenges for the New Astronomy (Berlin: Springer), 1013
Lampeitl, H., Smith, M., Nichol, R. C., et al. 2010, ApJ, 722, 566
Li, W., Leaman, J., Chornock, R., et al. 2011, MNRAS, 412, 1441

Mandel, K. S., Thorp, S., Narayan, G., Friedman, A. S., & Avelino, A. 2022, MNRAS, 510, 3939
Ménard, B., Nestor, D., Turnshek, D., et al. 2008, MNRAS, 385, 1053
Moreno-Raya, M. E., Mollá, M., López-Sánchez, Á. R., et al. 2016, ApJ, 818, L19
Pascale, M., Frye, B. L., Pierel, J. D. R., et al. 2024, arXiv:2403.18902
Perets, H. B., Gal-Yam, A., Mazzali, P. A., et al. 2010, Natur, 465, 322
Perlmutter, S., Aldering, G., Goldhaber, G., et al. 1999, ApJ, 517, 565
Pierel, J., Engesser, M., Bajaj, V., et al. 2024a, JWST Proposal. Cycle 3, ID. #5324
Pierel, J. D. R., Frye, B. L., Pascale, M., et al. 2024b, ApJ, 967, 50
Pierel, J. D. R., Jones, D. O., Kenworthy, W. D., et al. 2022, ApJ, 939, 11
Pierel, J. D. R., Newman, A. B., Dhawan, S., et al. 2024c, ApJL, 967, L37
Pierel, J. D. R., Rodney, S., Avelino, A., et al. 2018, PASP, 130, 114504
Polletta, M., Nonino, M., Frye, B., et al. 2023, A&A, 675, L4
Popovic, B., Brout, D., Kessler, R., & Scolnic, D. 2023, ApJ, 945, 84
Rest, A., Pierel, J., Correnti, M., et al. 2023, arminrest/jhat: The JWST HST Alignment Tool (JHAT), v2, Zenodo, doi:10.5281/zenodo.7892935
Rest, A., Stubbs, C., Becker, A. C., et al. 2005, ApJ, 634, 1103
Rieke, M., Robertson, B., Tacchella, S., et al. 2023, Data from the JWST Advanced Deep Extragalactic Survey (JADES), STScI/MAST, doi:10.17909/8TDJ-8N28
Riess, A. G., Filippenko, A. V., Challis, P., et al. 1998, AJ, 116, 1009
Riess, A. G., & Livio, M. 2006, ApJ, 648, 884
Riess, A. G., Rodney, S. A., Scolnic, D. M., et al. 2018, ApJ, 853, 126
Riess, A. G., Yuan, W., Macri, L. M., et al. 2022, ApJL, 934, L7
Rodney, S. A., Riess, A. G., Strolger, L.-G., et al. 2014, AJ, 148, 13
Rose, B. M., Baltay, C., Hounsell, R., et al. 2021b, arXiv:2111.03081
Rose, B. M., Rubin, D., Strolger, L., & Garnavich, P. M. 2021a, ApJ, 909, 28
Rubin, D., Hayden, B., Huang, X., et al. 2018, ApJ, 866, 65
Schlafly, E. F., & Finkbeiner, D. P. 2011, ApJ, 737, 103
Scolnic, D. M., Jones, D. O., Rest, A., et al. 2018, ApJ, 859, 101
Shen, K. J., Kasen, D., Weinberg, N. N., Bildsten, L., & Scannapieco, E. 2010, ApJ, 715, 767
Siebert, M. R., Decoursey, C., Coulter, D. A., et al. 2024, arXiv:2406.05076
Siebert, M. R., Foley, R. J., Jones, D. O., et al. 2019, MNRAS, 486, 5785
Siebert, M. R., Foley, R. J., Zenati, Y., et al. 2023, ApJ, 958, 173
Sullivan, M., Conley, A., Howell, D. A., et al. 2010, MNRAS, 406, 782
Sullivan, M., Kasliwal, M. M., Nugent, P. E., et al. 2011, ApJ, 732, 118
Taubenberger, S. 2017, in Handbook of Supernovae, ed. A. W. Alsabti & P. Murdin (Berlin: Springer), 317
Taubenberger, S., Hachinger, S., Pignata, G., et al. 2008, MNRAS, 385, 75
Tripp, R. 1998, A&A, 331, 815
Waldman, R., Sauer, D., Livne, E., et al. 2011, ApJ, 738, 21
Woosley, S. E., Taam, R. E., & Weaver, T. A. 1986, ApJ, 301, 601
Zenati, Y., Perets, H. B., Dessart, L., et al. 2023, ApJ, 944, 22